A MATLAB toolbox for computation of velocity and strain rate field from GNSS coordinate time series

Giordano Teza[*,1], Arianna Pesci[2], Marco Meschis[3]

[1] Alma Mater Studiorum University of Bologna, Department of Physics and Astronomy, Viale Berti Pichat 6/2, Bologna 40127, Italy

[2] Istituto Nazionale di Geofisica e Vulcanologia, Sezione di Bologna, Via Donato Creti, 12, 40128 Bologna, Italy

[3] Istituto Nazionale di Geofisica e Vulcanologia, Sezione di Palermo, via Ugo La Malfa, 153, 90146 Palermo, Italy

Abstract

We propose a MATLAB toolbox for the computation of the strain rate field from the coordinate time series of some continuous GNSS stations. It consists of several functions, also compatible with GNU Octave, implementing the following steps: (i) time series download from a data repository (e.g., the Nevada Geodetic Laboratory database); (ii) calculation of velocities of the selected stations by means of the Maximum Likelihood Estimation (MLE) method implemented in the external package Hector, including modeling of offsets, outliers, noise and periodic components; (iii) (optional) filtering of Common Mode Errors; (iv) calculation of the strain rate field with the modified least squares method, in which a scale factor can be introduced to define the locality of the deformation analysis and, besides uncertainty estimation, a geometric evaluation of the significance of the results is provided; (v) visualization of the results for immediate use and easy interpretation for scientific purposes. The toolbox is divided into two components: the first one, named StaVel, performs the steps (i)-(iii) and the second component, GridStrain, performs the steps (iv) and (v). The potential of the toolbox is demonstrated on a real dataset. Time series from several continuous GNSS stations in South-Eastern Sicily (Southern Italy) are processed by means of StaVel and GridStrain in order to provide the strain rate field.

Keywords: GNSS; Velocity; Crustal Kinematics; Crustal Deformations; Strain Rate Field

1. Introduction

Data continuously collected by means of a large number of well distributed Global Navigation Satellite System (GNSS) stations can be used for several purposes in geophysics and geodesy. The geophysical applications mainly focus on the estimation of relative displacements in order to investigate crustal tectonic deformations, whereas the main target in geodesy is the realization and maintenance of reference frames from national to global scales. However, the GNSS data are now processed and analyzed using harmonized strategies and standards in both geophysics and geodesy [Kenyeres et al., 2019]. In particular, nowadays there are several Continuously Operating Reference Stations (CORS) networks [Snay and Soler, 2008], which began to be constructed a few decades ago and

are still being developed today. Examples of regional CORS are EUREF in Europe [Legrand, 2022], with more than 300 stations, NCN (NOAA CORS Network) in the United States [NOAA National Geodetic Survey, 1994], with about 1900 stations, GEONET in Japan [Tsuji et al., 2017], with about 1300 stations, and many other all around the world. The combination of independent regional CORS data allows the creation of global-scale solutions for velocity and strain rate modeling [Kreemer et al. 2014; Kenyeres et al., 2019].

The Nevada Geodetic Laboratory (NGL) is a publicly available database which provides the 24h final solutions of about 20,000 stations distributed all along the world [Blewitt et al., 2018]. These time series are routinely processed by NGL by means of JPL GipsyX v1.0 software on the basis of several parameters such as nominal troposphere, troposphere delays models from VMF data server, elevation weighted observations, higher order ionospheric calibrations, improved JPL Repro 3 orbits, and the global reference frame IGS14. Moreover, the NGL data can also be provided, depending on the station position, in one or more plate reference frames defined using Euler rotation poles in accordance with Kreemer et al. [2014].

In order to improve the spatial coverage of the CORS networks, mainly by increasing the station density, cheaper episodic GNSS stations (epGNSS), on which measurements are periodically carried out with a campaign-style approach, are also used [Alothman et al., 2016; Kierulf, 2017]. Data provided by private GNSS networks built and maintained by cell phone carriers, with the aim of improving the corresponding positioning services, can also be successfully used to improve the coverage for purposes of crustal deformation monitoring, under the condition that an appropriate data quality control is carried out [Ohta and Ohzono, 2022].

A GNSS coordinate time series typically is a linear trend partly masked by periodic components (both geophysical signal and noise) and noise which can be estimated assuming the presence of white, flicker, and random walk noise [Williams et al., 2004]. If the time series are sufficiently long, at least 4.5 y, where y is the non-SI unit year, and adequate noise models are used, velocities from GNSS stations suitable geophysical and geodetic studies can be assessed [Masson et al., 2019]. In particular, Hector [Bos et al., 2013] is a free software package which allow, by means of a multi-step procedure, the recognition of offsets, such as (i) step discontinuities in the time series caused by equipment changes, earthquakes or other reasons, (ii) the outlier recognition and removal, (iii) the periodic noise and power law noise modeling and (iv) the velocity computation by means of the Maximum Likelihood Estimation (MLE) method [Langbein, 2004; Williams, 2008]. Offsets could lead to errors in velocity computation if not adequately faced [Williams, 2003]. However, although there are several algorithms for offset detection, the best algorithms are still overcome by the best expert eyeball [Gazeaux et al., 2013]. For this reason, Blewitt et al. [2016] proposed the Median Interannual Difference Adjusted for Skewness (MIDAS), which is an automatic velocity estimator aimed at mitigating the effects of seasonality and offsets by selecting data pairs separated by 1 year. In this way, even if some offsets are not recognized, their effects can be reduced.

Another possible cause of data perturbation, which can cause an increase in the uncertainty of the estimated velocities, is the Common Mode Error (CME). The CME mainly affects data of regional GNSS (some hundred kilometers) and is mainly due to reference frame error, mismodeling of satellite orbits and clocks and large-scale environmental effects [Gruszczynski et al., 2016]. The estimate of the CME, or in any case the identification of Common Mode Signals (CMSs), is particularly important in the case of the vertical component [Pintori et al., 2022], especially if the goal is to obtain a stable reference system. Currently, there are various methods for recognizing and removing possible CME, from stacking [Wdowinski et al., 1997] to more advanced methods such as variational bayesian principal component analysis [Li et al., 2020]. However, it should be emphasized that not all authors agree on the need to remove the common mode components because the CME could be accompanied by CMS [Pintori et al., 2022].

As reasonable estimates of the station velocities are available together with the corresponding uncertainties, the strain rate field can be computed on the nodes of a regular grid by means of a least squares (LS) approach. In order to evaluate a possible scale-dependent behavior of the studied system, or in any case to emphasize the effect of the stations as a function of the distance from the grid node where the calculation is performed as well as the uncertainty of the corresponding velocities, the modified LS (MLS) approach proposed by Shen et al. [1996] and Shen and Jackson [2000] can be used. It is based on the adjustment of LS covariance matrix by means of a chosen scale factor. The MATLAB implementation of MLS for the strain rate field calculation on a grid (grid_strain) or on a 2.5D digital model referred to a grid (grid_strain3) is proposed by Teza et al. [2008].

In this paper, we propose a MATLAB toolbox aimed at computing velocities and strain rate from GNSS position time series. The input data are coordinate time series and a function allows the direct download from NGL, according to a station list (the user can use another data repository, if necessary). As the data are downloaded, a function calls

the free software Hector (Bos et al, 2013) to carry out the MLE-based velocity estimation (Hector must be separately downloaded and installed). Finally, a strongly revised and improved version of grid_strain performs the MLS-based computation of the strain rate. This toolbox is conceived in order to offer a free package that can provide the strain rate field in a highly automated way (although the offset research stage, if the user prefers this, can be implemented manually), also including visualization tools that can facilitate the interpretation of the results. The toolbox can be used for many geodetic investigations in geophysics, including plate tectonics and estimation of strain across faults systems. It can be downloaded from the HARVARD data repository.

2. Workflow and implementation

The implemented procedure is structured according to the following steps (Figure 1):

■ Download of the time series of the selected GNSS stations from a data repository or, alternatively, access to a database of time series. Availability of time series obtained by RINEX data processing is a precondition for the procedure described here.

■ For each coordinate time series of each station, these operations are carried out:
  – offset recognition or importation from a database;
  – outlier recognition and modeling;
  – MLE-based velocity computation;
  – (optional) CME filtering.
  In particular, for each station these files are generated:
  – Four or six ASCII .mom files, where mom states for Modified Julian date, Observations, Model, for each component: (i) raw time series; (ii) observation time series after offset recognition/importation; (iii) preprocessed time series after outlier removal; (iv) model time series after trend estimation and, optionally, (v) CME-filtered preprocessed time series and (vi) CME-filtered model time series;
  – a MATLAB object of tsData class (this object is described in detail in Chapter 3).

■ For the whole area:
  – use of the estimated trends in order to obtain the set of station velocity vectors;
  – (optional, if the CME estimation and filtering are carried out): CME estimation;
  – generation of a regular grid;
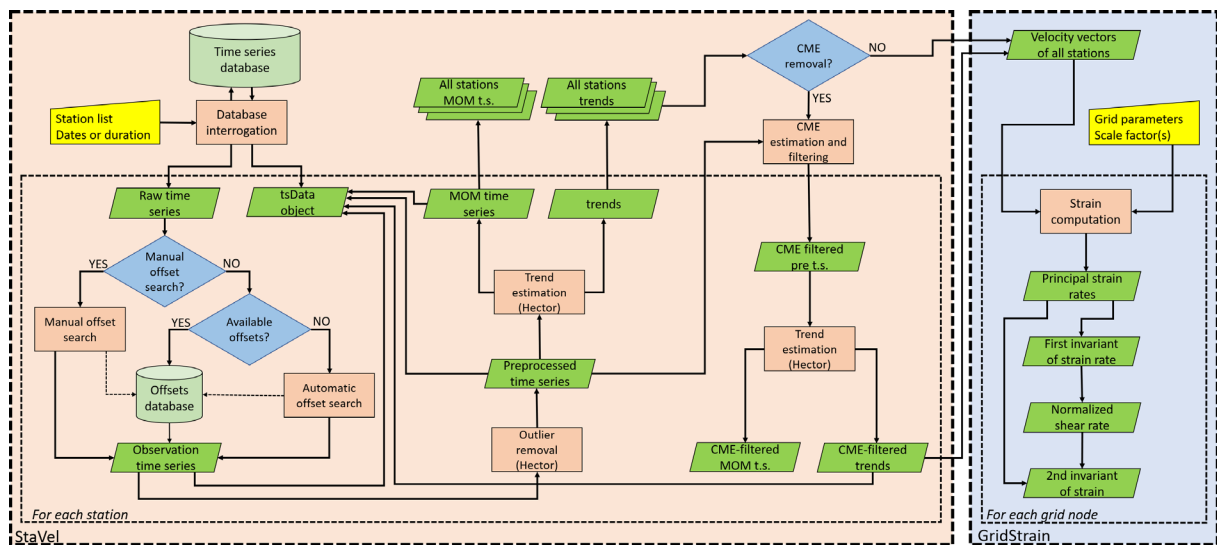 – choice of one or more scale factors.

Figure 1. Workflow of the method. The two rectangles with a colored background collect and show the steps implemented in StaVel and GridStrain respectively. The two internal rectangles highlight the steps implemented for each station (StaVel) and for each node of the grid (GridStrain).

- ■ For each node of the regular grid:
  - – strain rate field computation with the MLS method for one or more scale factors, including the computation of first and second invariant of the strain and of normalized shear;
- ■ Visualization and interpretation of the results.

The proposed toolbox actually has two components, the first one (StaVel) for the calculation of the velocities and the second one (GridStrain) for the calculation of the strain field. Although the toolbox is designed to use both components in succession, to calculate a strain field it is sufficient to have an ASCII file of the required format, as shown in the GridStrain user's guide. Each component consists of several MATLAB scripts and functions and, in the case of StaVel, calls an external package (Hector). The links for the download of the two components are shown in Section 5 ("Data and sharing resources").]

The length of a time series is crucial and affects the estimation of strain rate. In particular, the minimum time series length should be 4.5 y to have reasonable results, even if an 8 y length is recommended to keep the uncertainties within 0.2 mm/y and 0.5 mm/y for the horizontal and vertical velocity components, respectively. Moreover, Serpelloni et al. [2022] showed that, in order to obtain results which are statistically consistent with velocity estimates obtained from time-series longer than 10 y, lengths of ~6 y and ~7 y are required for horizontal and vertical components respectively. For this reason, besides the station list, also the dates and/or the minimum time series duration are input data of the calculation process.

2.1 Velocity estimation

Because of plate movement and other geophysical phenomena, each component of the coordinate daily time series of a GNSS station is generally modelled as a linear trend plus seasonal components and noise. In the case of the East component $E(t)$ (the same considerations apply to the North and vertical components $N(t)$) and $V(t)$ respectively), at a time t_k it is [Langbein, 2020]:

$$E(t_k) = E_0 + v_E(t_k - t_0) + \sum_{l=1}^{L} o_{El} H(t_k - t_l) + \sum_{m=1}^{M} [s_{Em} \sin(2\pi f_m t_k/365.25) + c_{Em} \cos(2\pi f_m t_k/365.25)] + n_{Ek}, \quad (1)$$

where:
- – $k = 0,1,\cdots,N_t - 1$, where N_t is the time series length in days;
- – E_0 is the position at time t_0; v_E is the velocity;
- – $H(t)$ is the Heaviside step function, i.e. $H(t) = 0$ for $t \le 0$ and $H(t) = 1$ for $t > 0$;
- – o_{El} is the size of the l-th offset occurring at time t_l;
- – s_{Em} and c_{Em} represent the periodic terms at the frequency f_m, typically it is $M = 2$, with $f_1 = 1$ cpy, related to the yearly component (cpy is the non-SI unit cycles per year), and $f_2 = 2$ cpy, related to the half-yearly component. The draconitic component at $f_D = 1.04$ cpy can also be considered together with some related harmonics [Ray et al., 2004], but it is generally treated as CME because it is a periodic noise;
- – n_{Ek} is a random variable representing the noise, which is typically modeled as the sum of white noise, colored noise, i.e. noise whose spectral density per unit of frequency bandwidth is proportional to $f^{-\beta}$ ($\beta = 1$: flicker noise, or pink noise; $\beta = 2$: random walk noise, or Brown noise), or also Gauss-Markov noise or band-pass-filtered noise.

If the velocity changes with the time, Eq. (1) becomes

$$E(t_k) = E_0 + v_{E0}t_k + \sum_{n=1}^{N} v_{En}(t_k - t_n)H(t_k - t_n) + \sum_{l=1}^{L} o_{El}H(t_k - t_l) +$$

$$+ \sum_{m=1}^{M} [s_{Em} \sin(2\pi f_m t_k/365.25) + c_{Em} \cos(2\pi f_m t_k/365.25)] + n_E, \quad (2)$$

where v_{E0} is the initial velocity and v_{En} is the velocity change occurred at the time t_n.

The main aim of the data analysis is the estimation of velocity and corresponding standard deviation (SD). To obtain this, all coefficients in Eq. (1) or (2) must also be estimated. An MLE-based approach is aimed at solving the matrix equation:

$$\mathbf{y} = A\mathbf{x} + \mathbf{r}, \tag{3}$$

where A is the design matrix, which contains data about trend, bias, seasonal signals and offsets, $\mathbf{x} = [E_0, v_E, o_{El}, s_{Em}, c_{Em}]$ (or $\mathbf{x} = [E_0, v_E, v_{En}, o_{El}, s_{Em}, c_{Em}]$) is the vector of unknowns to be estimated and $\mathbf{r} = \mathbf{y} - A\hat{\mathbf{x}}$ is the residual, with $\hat{\mathbf{x}}$ estimate of $\mathbf{x}$ (same considerations for North and Vertical component). The solution is obtained by optimizing the covariance matrix, which is based on chosen noise models, by means of likelihood function maximization. This optimization process also provides estimates of the standard deviations of the noise components included in the modeling. Examples of free software for GNSS time series modeling are CATS [Williams et al., 2008] and Hector [Bos et al., 2013]. In particular, Hector is attractive because it has good performance, it can be easily operated by means of MATLAB, also thanks to the generation of JSON (JavaScript Object Notation) files with the results for each calculation step, and, last but not least, it is periodically upgraded (download page: http://segal.ubi.pt/hector/). For these reasons, Hector is directly called, when necessary, by StaVel, i.e. the component of the proposed toolbox devoted to velocity estimation.

There are some data that should be known when the MLE modeling is carried out, i.e. the possible offset times t_l and the possible velocity change times t_n. This because the coefficients o_l in Eqs. (1), (2) and/or v_n in Eq. (2) are estimated, but the corresponding times should be known. An example of effects of unmodeled offsets can be found in Figure 2. The specific station is CUTR (Cutro, Southern Italy [Meschis et al., 2020]) and the MLE-based velocity estimates are $v_E = 2.66 \pm 0.10$ mm/y, $v_N = 1.84 \pm 0.16$ mm/y and $v_V = 5.7 \pm 0.7$ mm/y for the East, North and vertical component respectively if the offsets are not recognized and modeled. The MLE-based velocity estimates are $v_E = 2.75 \pm 0.16$ mm/y, $v_N = 3.68 \pm 0.14$ mm/y and $v_V = 0.3 \pm 0.5$ mm/y instead in the case where the occurred offset is recognized in a manual way and correctly modeled (by way of comparison, the corresponding MIDAS velocities downloaded from the NGL data repository are $v_E = 2.94 \pm 0.26$ mm/y, $v_N = 3.89 \pm 0.30$ mm/y, $v_V = 1.4 \pm 1.0$ mm/y). Within Hector there is a program for the offset detection. However, the offsets can also be detected in a manual way because the performance of available algorithms for automatic detection is not always adequate [Gazeaux et al., 2013]. Information about offsets can be found in some data repository. For example, NGL database also provides offsets due
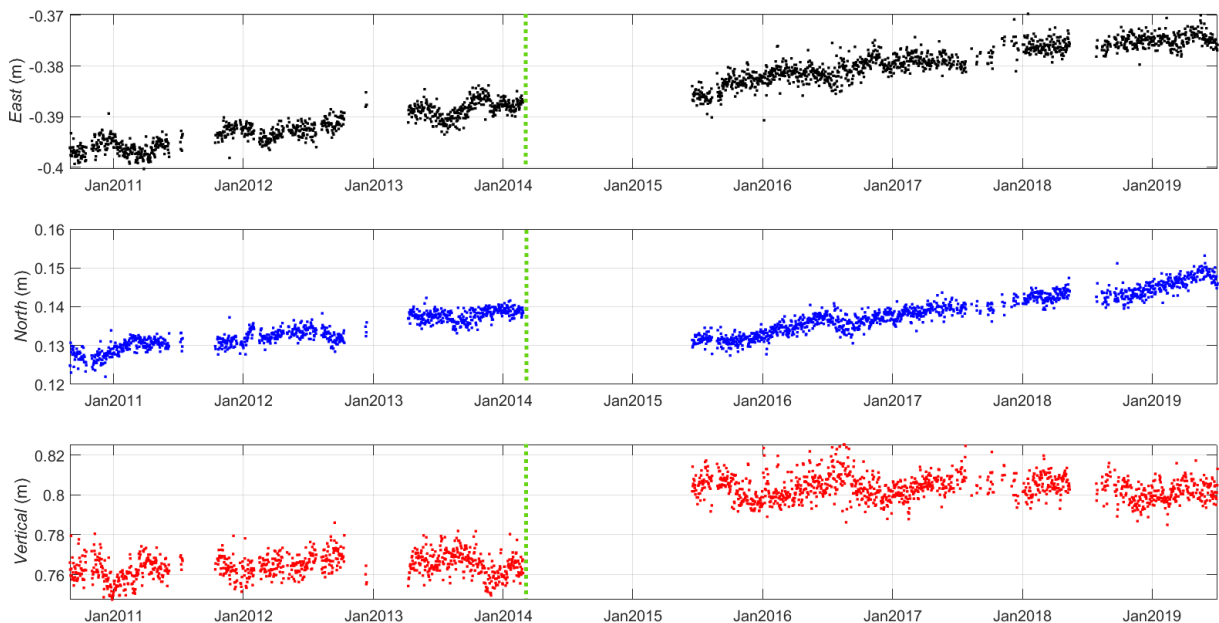

Figure 2. Example of case where significant offsets occur. The offset date corresponds to the vertical dotted line. If the offset is unmodeled, the relative error is 3% and 50% for the East and North component respectively, whereas the estimated velocity is even an order of magnitude greater than the true one for the vertical component.

to antenna change, receiver change, other changes or also near earthquakes. StaVel can directly download data from this database. A user could also upgrade his/her offset database with the results of automatic or manual offset search.

Another important stage before velocity estimation is the recognition and removal of outliers. If this stage is not carried out, in some conditions significant errors could affect the velocity estimates. Currently, there are several high-performance algorithms which can be advantageously used such as the three-sigma method (3σ) [Mao et al., 1999], the Median Absolute Deviation, MAD [Klos et al., 2015] and the wavelet analysis [Ji and Shen, 2020]. The Hector component aimed at recognizing and removing outliers uses high-pass filtering applied to time series and removes the measurements that fall outside N times the interquartile range (IQR), where $N = 3$ is generally chosen [Langbein and Bock, 2004].

The last step of the velocity calculation procedure is based on the MLE algorithm. Before the velocity calculation, the noise models are to be chosen. White noise and flicker noise are generally observed in the time series and, therefore, the corresponding models should be introduced in the calculation [Ray et al., 2008]. It is also important to note that random walk noise is also often found [Dmitrieva et al., 2015]; therefore, this model should also be considered. Hector allows several possible choices about the noise models, as shown in the corresponding user's guide. For the i-th GNSS station ($i = 1, 2, \cdots, S$, where S is the number of processed stations), whose position is $\mathbf{x}_i = [E_i, N_i, V_i]$ expressed in a convenient Universal Transverse Mercator (UTM) zone, the results are the velocity vector $\mathbf{v}_i = [v_{Ei}, v_{Ni}, v_{Zi}]$ and the corresponding SDs σ_{vEi}, σ_{vNi} and σ_{vZi}. It is important to note the fact that in subsequent calculations the velocity uncertainties are as relevant as the values of the corresponding quantities. Moreover, often no more than the two horizontal coordinates are considered. As the computations are finalized, it is generated a text file with the station names, UTM coordinates, velocities and velocity uncertainties, which can be used to estimate the strain rate by using GridStrain.

If the user intends to estimate and reduce the CME, four approaches are offered within StaVel: (i) stacking [Wdowinski et al., 1997]; (ii) weighted stacking [Nicolaidis, 2002]; (iii) distance weighted stacking [He et al., 2020] and (iv) correlation weighted stacking [Tian and Shen, 2011]. A more advanced method, including a procedure for frequency domain discrimination between CME and common mode signals, is being developed and tested and will be added in a future upgrade of the toolbox. To briefly explain the equations used, the case of the East component is shown here; the same considerations apply to the North and Vertical components. A preliminary step is the generation of synchronized daily time series by introducing NaN (not-a-number) values where data, i.e. coordinate time series, are missing. For each station, detrending is then performed on the basis of the previously estimated velocity and, considering the presence of any offsets, the time series is shifted so as to have zero average, thus obtaining the residual time series. Since some researchers prefer to detrend using models with a low number of parameters [e.g. Pintori et al., 2022], a simple line least squares fitting to a straight line is also available. Let $\varepsilon_{Ei}(t_k)$ be the residual time series of East coordinates for the i-th station. The East CME at the time t_k is computed in the cases (i)-(iii) in this way:

$$CME_E(t_k) = \sum_{i=1}^{Ns} \mu(t_k)\eta_i(t_k)w_{Ei}(t_k)\varepsilon_{Ei}(t_k) \bigg/ \sum_{k=1}^{Ns} \mu(t_k)\eta_i(t_k)w_{Ei}(t_k), \tag{4}$$

where $\mu(t_k) = 1$ if there are data for at least three stations (or a number higher than 3 defined by the user) at the time t_k and $\mu(t_k) = 0$ otherwise, $\eta_i(t_k) = 1$ if $E_i(t_k)$ is numeric and $\eta_i(k) = 0$ if $E_i(t_k)$ is NaN, $w_{Ei}(t_k) = 1$ for each i and k for the simple stacking, $w_{Ei}(t_k) = 1/\sigma_{Ei}^2(t_k)$ for the weighted stacking ($\sigma_{Ei}(t_k)$ is the SD of the East time series at t_k), and $w_{Ei}(k) = 1/d_i^2$ for the distance weighted stacking (d_i is the distance of the station i from the center of the GNSS network). In these cases, a $N_t \times 1$ vector $\mathbf{CME}_E$ is obtained; this vector is used for the CME filtering of all stations. For the correlation weighted stacking the weights are $w_{Eij}(t_k) = r_{Eij}/\sigma_{Ei}^2(t_k)$, where r_{Eij} is the correlation coefficient between the residual time series of stations i and j. The equation becomes

$$CME_{Ej}(t_k) = \sum_{i=1}^{Ns} \mu_i(t_k)w_{Eij}(t_k)\varepsilon_{Ei}(t_k) \bigg/ \sum_{k=1}^{Ns} \mu_i(t_k)w_{Eij}(t_k), \tag{5}$$

leading to a $N_t \times S$ matrix CME_E whose column j is the CME to be used for the filtering of the East time series of the station j. After the CME filtering, Hector is called again in order to provide a new velocity estimate. Examples

of time series of a real station (HLNI, i.e. Lentini, Syracuse, Italy) before and after CME filtering, and corresponding models according to Eq. (1) with white noise and power law noise, are shown in Figure 3.
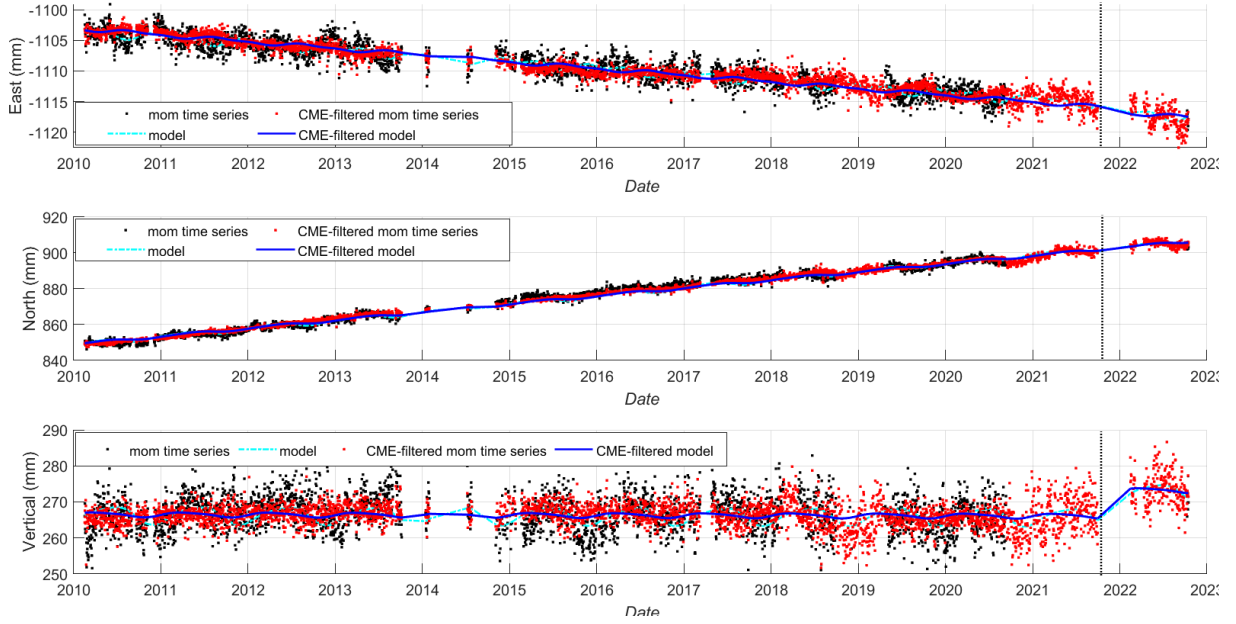

Figure 3. Example of mom time series, i.e. time series after the trend modeling, and mom time series after covariance-weighted CME filtering, and corresponding models for the HLNI station. When the CME cannot be estimated due to the small number of nearby stations (e.g. after 9 September 2021), the time series coincide. Moreover, an offset occurred on 16 October, 2021 (vertical dotted line).

2.2 Strain rate field estimation

The second component (GridStrain), which is aimed at computing the strain rate field, is an evolution of grid_strain [Teza et al., 2008]. The strain rate field is computed on the nodes of a chosen regular grid (or on the points of a Digital Terrain Model, DTM, which is a 2.5D digital model referred to regular grid). For simplicity, the 2D case is briefly described here; see Teza et al. [2008] for more details about the theory. Let $\mathbf{v} = [v_{E1}, v_{N1}, v_{E2}, v_{N2}, \cdots, v_{ES}, v_{NS}]^T$ be the vector of estimated velocities of the S stations, where ^{T} indicates the vector transposition. For the grid node hk ($h = 1,2,\cdots,n_N$, $h = 1,2,\cdots,n_E$, where n_N and n_E are the numbers of grid rows and grid columns respectively), the matrix equation

$$\mathbf{v} = A_{hk}\mathbf{l}_{hk}, \tag{6}$$

where A_{hk} is the specific design matrix and $\mathbf{l}_{hk}$ is the vector of parameters to estimate, is solved in a LS sense. The matrix A_{hk} encodes the distances between the S stations and this grid node, whose coordinate vector is $\mathbf{x}_{hk} = [x_{hk}, y_{hk}]$, where $x_{hk} = x_{11} + (k-1)\Delta_E$, $y_{hk} = y_{11} + (h-1)\Delta_N$, x_{11} is the minimum grid Easting, y_{11} is the minimum grid Northing, and Δ_E, Δ_N are the East and North grid steps respectively (the usual choice is $\Delta_E = \Delta_N$). The estimated vector $\mathbf{l}_{hk} = [V_x, V_y, L_{xx}, L_{xy}, L_{yx}, L_{yy}]^T$ shows the velocities along East and North and, above all, the matrix elements of the velocity gradient tensor $\mathbf{L}_{hk} = [L_{xx}, L_{xy}, L_{yx}, L_{yy}]^T$.

In a standard LS computation of $\mathbf{l}_{hk}$, (for simplicity, the grid node indexes hk are omitted later on), under the hypothesis that the velocity uncertainties are uncorrelated, the covariance matrix

$$W_{hk} = \sigma_D^{-2}\text{diag}(\sigma_{E1}^{-2}, \sigma_{N1}^{-2}, \sigma_{E2}^{-2}, \sigma_{N2}^{-2}, \cdots, \sigma_{ES}^{-2}, \sigma_{NS}^{-2}) \tag{7}$$

is used, where σ_D^2 is the mean of velocity variances. In such a calculation, the effect of the ith station is weighted with the corresponding inverses of variances σ_{Ei}^{-2} and σ_{Ni}^{-2}. A station with low velocity SDs matters more than a station with higher velocity SDs. The key of MLS is the multiplication of the weights of the ith station by a decreasing continuous function $f(d_i/d_0)$, called scaling function, where $d_i = \|\mathbf{x}_i - \mathbf{x}_{hk}\|$ and d_0 is a fixed value, called scale factor, i.e. the weights σ_{Ei}^{-2} and σ_{Ni}^{-2} become $f(d/d_0)\sigma_{Ei}^{-2}$ and $f(d/d_0)\sigma_{Ni}^{-2}$ respectively. In this way, the stations closest to the node are more important in LS calculations and those that are at a distance greater than d_0 are progressively less important. Shen and Jackson (2000) proposed the scaling function $\exp(-d/d_0)$, but other functions can be considered. The new toolbox allows the choice between exponential, Gaussian, i.e. the function $\exp\{-(d/d_0)^2\}$, which strongly reduces the effect of distant stations, and inverse square $1/[1 + (d/d_0)^2]$, which on the contrary slightly attenuates the effect of the scale factor (Figure 4).
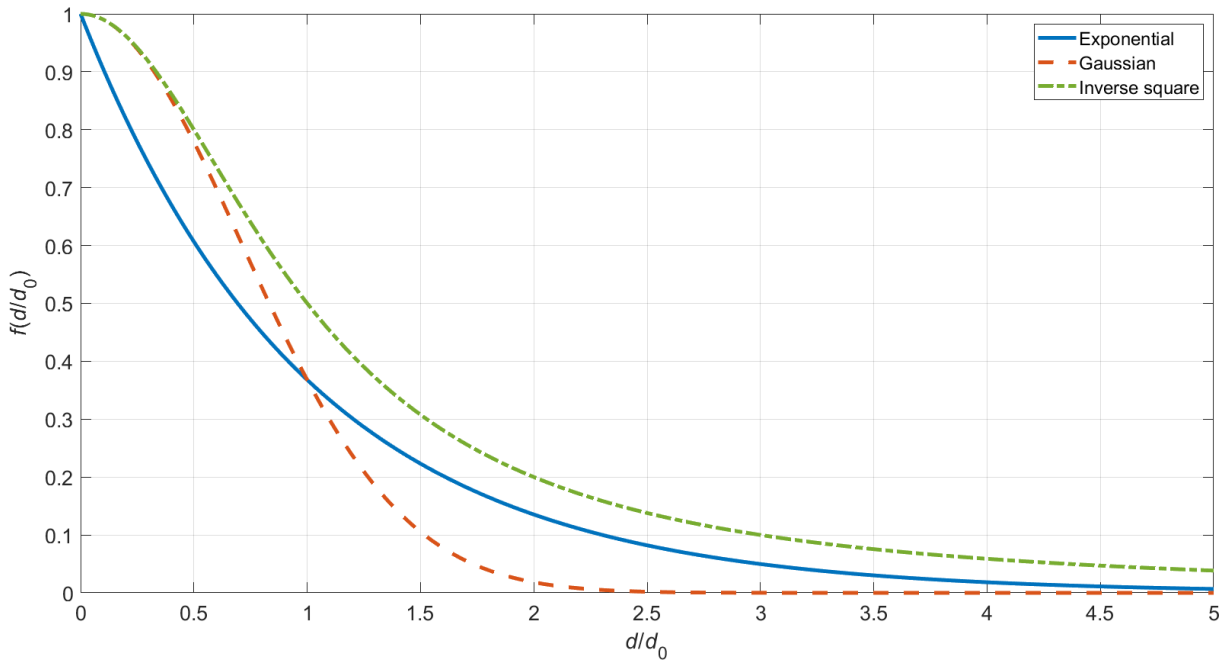

Figure 4. Scaling functions available in the proposed MATLAB toolbox.

As the velocity gradient tensor L is estimated, its symmetric part, which is the strain rate tensor

$$\dot{\mathrm{E}} = \begin{bmatrix} \dot{\varepsilon}_{xx} & \dot{\varepsilon}_{xy} \\ \dot{\varepsilon}_{xy} & \dot{\varepsilon}_{yy} \end{bmatrix} \tag{8}$$

and represents the rate of internal deformation, and its antisymmetric part, which represents a rigid body motion, are obtained.

The toolbox provides, for each grid node:

(i) the strain rate represented by the maximum and minimum principal strain rates $\dot{\varepsilon}_{max}$ and $\dot{\varepsilon}_{min}$, eigenvalues of $\dot{\mathrm{E}}$, and by the directions of the corresponding eigenvectors. The uncertainties of $\dot{\varepsilon}_{max}$ and $\dot{\varepsilon}_{min}$ are also provided;

(ii) the first invariant of the strain rate tensor (dilatation rate, or rate of change in area; change in volume in the 3D case), i.e. the trace of the strain rate tensor $\dot{\varDelta} = \dot{\varepsilon}_{xx} + \dot{\varepsilon}_{yy} = \dot{\varepsilon}_{max} + \dot{\varepsilon}_{min}$;

(iii) the engineering shear rate $\dot{\gamma} = \dot{\varepsilon}_{max} - \dot{\varepsilon}_{min}$ normalized to $\dot{\varDelta}$, i.e. $\dot{\gamma}/\dot{\varDelta}$;

(iv) the second invariant of the strain rate $\sqrt{\dot{\varepsilon}_{xx}^2 + \dot{\varepsilon}_{yy}^2 + 2\dot{\varepsilon}_{xy}^2} = \sqrt{\dot{\varepsilon}_{max}^2 + \dot{\varepsilon}_{min}^2}$;

(v) the geometric significance of the results;

(vi) translation and rotation;

(vii) (only in 3D case), the Flinn's k-value.

The rates $\dot{\Delta}$ and $\dot{\gamma}$ allow the recognition of the zones of the studied area characterized by different behavior. The rate $\dot{\Delta}$, which neglects nature and geometry of the strain tensor, allows an evaluation of the deformation pattern inside an area having a specific behavior (extensional or compressional) to be determined. The rate $\dot{\gamma}/\dot{\Delta}$, which also provides information on the sign of both the principal strains, allows the recognition of the boundaries between areas characterized by different kinematics. The second invariant represents the magnitude of total strain rate. As concerns the geometric significance, the results in a grid node are considered to have high, mean and low significance if the stations are distributed, within the scale factors, in all four quadrants, no more than three quadrants, and no more than two quadrants respectively. Finally, the k-value represents the shape of the strain ellipsoid ($k < 1$: flattening; $k > 1$: constriction; $k = 1$: planar strain).

GridStrain differs from grid_strain for the following reasons:
  (i) the main functions are of the object-oriented type;
 (ii) user interface controls are now used instead of menu of choices;
(iii) three possible scaling functions can be used and a user-defined scaling function can also be used;
(iv) a background map can be used to provide the results, avoiding the postprocessing of the figures with other software packages;
  (v) the station names can now be managed;
(vi) new visualization functions are now available (for example, the second invariant of the strain rate is now available);
(vii) the results of calculations and visualizations can be exported as Esri ASCII raster .asc files, therefore compatible with GIS software packages.

As in the case of grid_strain, it is possible to exclude one or more stations from the calculation of the strain rate field (for example, stations affected by peculiar motions such as landslides can be excluded, or the user can evaluate the effect of the exclusion of some stations). The excluded stations are highlighted with different color in the strain rate maps.

2.3 Other details on the MATLAB implementation

The main functions have user interface controls to facilitate their interactive use. Since no specific official MATLAB toolboxes are invoked, the toolbox is compatible with GNU Octave (however, in this case some functions must be called by means of command lines because some interface controls do not work). As mentioned, Hector is outside MATLAB and must be separately downloaded and installed. Moreover, Hector runs under Linux regardless to the operating system (OS) used by MATLAB. If the OS is Windows, the automatic Hector call by MATLAB requires the Windows Subsystem for Linux 2 (WSL2).

In general, the main MATLAB functions of the toolbox are developed using object-oriented programming. Some objects defined in MATLAB are used in order to facilitate the execution and possible future updating of the procedures, as well as their possible translation into Python. In some cases, a structure variable is used like an object. For example, a structure variable, generated by means of a function, allows the management of options for each stage of velocity computation (data folders, options about noise models, other parameters). In particular, the control files for Hector are generated on the basis of such a structure variable.

For each chosen continuous station, a tsData object is generated and upgraded during the velocity calculation. In the current version, a tsData object can be generated with the raw time series taken from a .tenv3, .tenv or .kenv ASCII files provided by NGL (please see http://geodesy.unr.edu/gps_timeseries/README_tenv3.txt for .tenv3 and corresponding links for .tenv and .kenv files), or from a .pos time series ASCII file provided by INGV. The functions that extracts these data from the input ASCII files are methods of this object. Since all .m files are available to the user, he/she can make the toolbox compatible with other kinds of input files by editing the tsData.m file and modifying a method or also adding other methods to tsData. The properties of an object of tsData class are related to either the input time series or the time series processing (in this second case, no tsData methods are used, but the object itself is upgraded at each stage, as shown in Figure 1). More details on objects of tsData class can be found on the User's Guide or can be obtained by typing help tsData on the MATLAB Command Window (MCW).

The first component, i.e. StaVel, can be used in several ways. To clarify the matter, the general option that appears when starting the program is shown in Figure 5. The user can perform all the velocity computation stages in a completely automatic way, including generation of tsData and .mom files, offset search, outlier removal, trend estimation and including or excluding the CME estimation and removal (if the CME is removed, the trend is re-estimated).
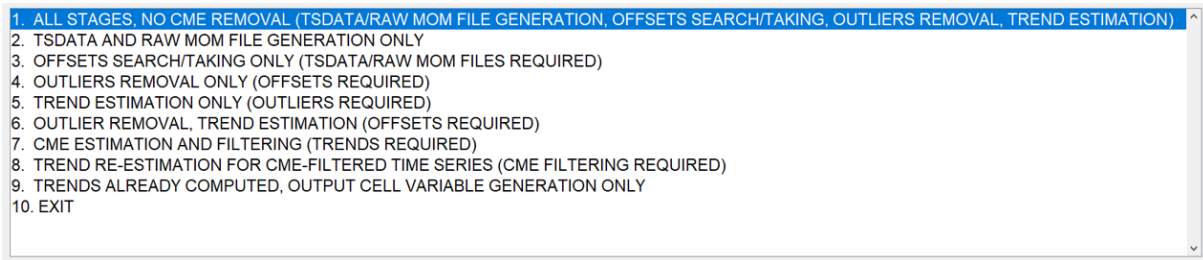
1. ALL STAGES, NO CME REMOVAL (TSDATA/RAW MOM FILE GENERATION, OFFSETS SEARCH/TAKING, OUTLIERS REMOVAL, TREND ESTIMATION)
2. TSDATA AND RAW MOM FILE GENERATION ONLY
3. OFFSETS SEARCH/TAKING ONLY (TSDATA/RAW MOM FILES REQUIRED)
4. OUTLIERS REMOVAL ONLY (OFFSETS REQUIRED)
5. TREND ESTIMATION ONLY (OUTLIERS REQUIRED)
6. OUTLIER REMOVAL, TREND ESTIMATION (OFFSETS REQUIRED)
7. CME ESTIMATION AND FILTERING (TRENDS REQUIRED)
8. TREND RE-ESTIMATION FOR CME-FILTERED TIME SERIES (CME FILTERING REQUIRED)
9. TRENDS ALREADY COMPUTED, OUTPUT CELL VARIABLE GENERATION ONLY
10. EXIT

Figure 5. Initial option for the first component (StaVel) of the proposed toolbox.

The toolbox is designed in such a way that it can work with a high level of automation. Obviously, there are some functions aimed at inspecting data and results at various stages of the processing, in order to evaluate, in particular, the effect of offset recognition, trend modeling and, when necessary, CME filtering.

3. Application to a case study

In order to show how the toolbox operates in a real case, the 2D deformation pattern of South-Eastern Sicily is studied and interpreted on the basis of the known geology.

3.1 Geological setting

The investigated area, lying within the Hyblean Plateau (HP), is affected by the ~N-S Neogene to Quaternary tectonic convergence between the African and Eurasian continental margins [e.g. Faccenna et al., 2001]. In particular, the HP identifies the onshore sector of a larger foreland domain, belonging to the Pelagian Block, and represents a carbonate promontory of the larger African palaeomargin [e.g. Grasso and Lentini, 1982; Meschis et al., 2020]. Seismic and geological investigations have uncovered a 5-6 km-thick Meso-Cenozoic sedimentary carbonate succession with intercalated volcanic layers, which overlie the Palaeozoic basement; in places Quaternary marine deposits associated with sequences of raised marine terraces overlie the before-mentioned Meso-Cenozoic rock succession [Bianca et al., 1999; Lentini et al., 1987; Meschis et al., 2020]. Neogene tectonic continental convergence and the associated crust shortening has affected the northern margin of the Pelagian Block producing a NE-SW oriented SE-verging thrust and fold system to the northwest and normal faulting on the HP [e.g. Cultrera et al. 2015; Grasso et al. 1995; Meschis et al. 2020]. NNW oriented continental convergence is currently accommodated by a regional-scale, northward deepening crustal seismogenic structure named here Main Thrust Fault (MTF), Figure 6, and also well-known as Sicilian Basal Thrust. This agrees with (i) focal mechanism showing a nearly N-S convergence and (ii) some field evidence of active folding and thrusting crustal deformation at the Sicilian Chain front identified on the northern rim of the HP [e.g. Lavecchia et al., 2007; Meschis et al., 2020]. Indeed, this region is thought to be seismically active yet it only partially accommodates the active convergence between Eurasia and Africa, measured using GNSS system along an ideal N-S oriented transect in SE Sicily [e.g. Mastrolembo Ventura et al., 2014; Meschis et al., 2020; Musumeci et al., 2014; Palano et al., 2012; Palano, 2015].

Within the investigated area there are 18 GNSS stations whose time series are at least 4.5 y long. The main data, i.e. coordinates in WGS84 UTM33N reference frame, velocities in direction East and North (v_E and v_N respectively) and corresponding SDs (σ_E and σ_N respectively) in the Eurasian Plate (EU), are summarized in Table 1. The station locations are shown in Figure 6.

3.2 Results and interpretation

The velocity vectors obtained by means of StaVel, including the 2-sigma error ellipses, are shown in Table 1 and Figure 6. The StaVel input data, i.e. the time series used for this study, are the 24h final solutions available at NGL database [Blewitt el al., 2018]. They were processed by NGL by means of JPL GipsyX v1.0 software on the basis of
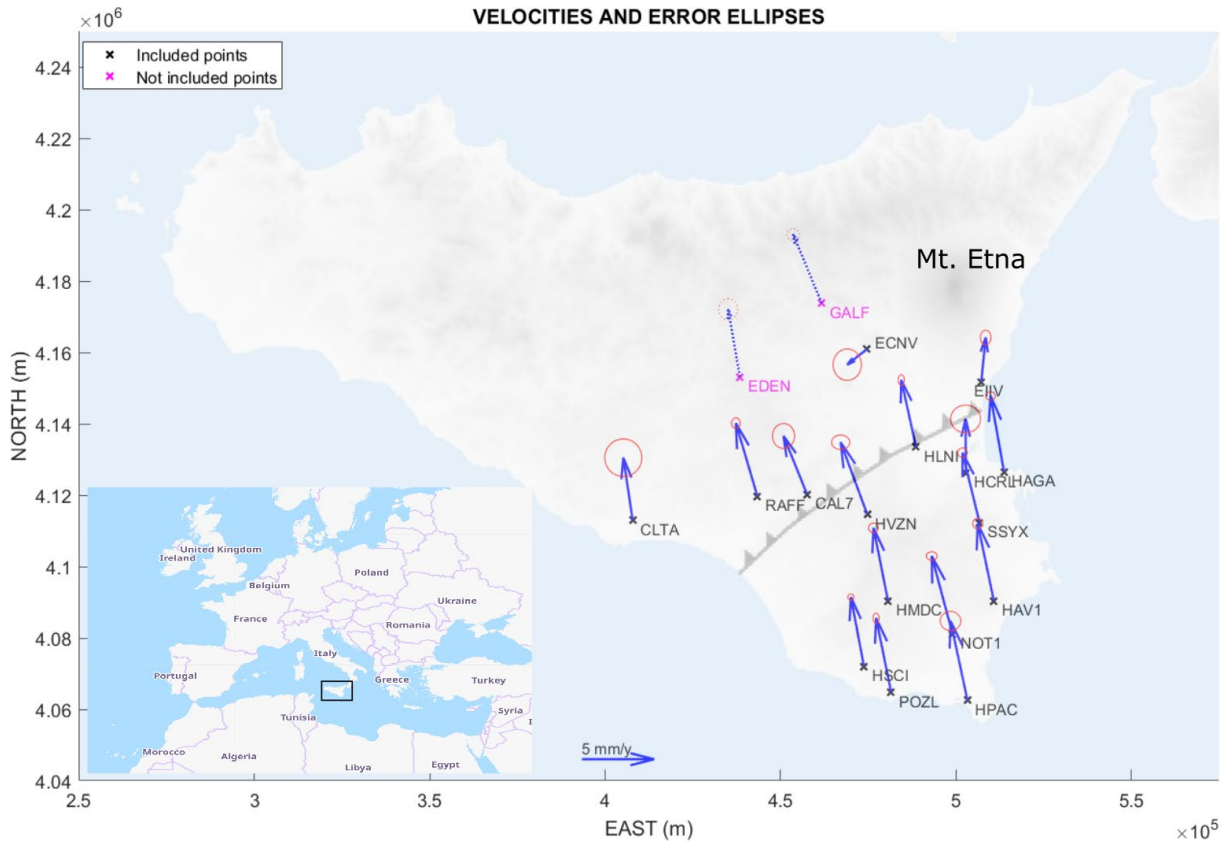
Figure 6. Sicily map, GNSS station positions and corresponding velocities (EU plate) with 2-sigma error ellipses (used stations: solid arrows; not used stations: dotted arrows). The Main Thrust Front (MTF) is also shown with the black line and triangles. For the Europe map, © OpenStreetMap contributors. The georeferenced background image is generated by means of a StaVel function from OpenTopography free SRTM DTM data [Farr et al., 2007].

several parameters such as nominal troposphere, troposphere delays models from VMF data server [Boehm et al., 2006], elevation weighted observations, higher order ionospheric calibrations, improved JPL Repro 3 orbits and the global reference frame IGS14. The plate rigid motion is removed using the Euler poles defined in Kreemer et al. [2014].

Regarding offsets, NGL information was used, visually verified and then manually integrated where necessary (the implementation of automatic offset recognition proved unsatisfactory with the available data). The recognition of the outliers and all the other operations aimed at calculating the speeds were performed automatically, even if they were visually verified at the calculation end.

The strain rate tensors in the high (solid lines) and mid significance (dotted lines) grid nodes, computed by means of GridStrain with 7.5 km grid side, 28 km scale factor and exponential scaling function, are shown in Figure 7a, where positive values indicate extensions (blue arrows) and negative values indicate compression (red arrows). In general, the behavior is mainly convergent, as highlighted by the map of change in area rate (Figure 7b). The map of normalized shear rate shows that the local crustal kinematics is controlled by MTF (Figure 7c). Finally, the map of the second invariant highlights the magnitude increase of the strain rate along the MTF from east to west (Figure 7d). This is not surprising taking into account that crustal shortening due to tectonic convergence between African and Eurasian plates is partially accommodated along the NE-SW oriented MTF.

The main results obtained for three scale factors, i.e. 28 km, 24 km and 20 km, are summarized in Table 2, where five zones are considered with respect to MTF:

(i) the North-East one (NE), where there are the stations ECNV, EIIV and HLNI (stations EDEN and GALF are excluded from computations because of velocity changes occurred in 2015 and 2018). This area is characterized by significant mostly N-S oriented compression (azimuth of the first eigenvector in the range 75-85°) because velocities of HAGA, HCRL, HVZN and SSYX in this direction are significantly higher than the NE ones. The compression, which prevails on extension on the orthogonal direction by a factor 3-4, reaches 140 nstrain/y, where nstrain is the non-SI unit, actually a dimensionless quantity, 10^{-9};

Station	Used	Site[1]	Coordinates WGS83 UTM33N		Velocities EU plate			
			East (m)	North (m)	V_E (mm/y)	σ_E (mm/y)	V_N (mm/y)	σ_N (mm/y)
CAL7	Y	Caltagirone (CT)	457593.72	4120307.36	–1.63	0.19	3.97	0.21
CLTA	Y	Licata (AG)	407892.85	4112966.74	–0.65	0.32	4.27	0.32
ECNV	Y	Centuripe (EN)	474617.70	4160988.03	–1.35	0.24	–1.06	0.27
EDEN	N[2]	Enna	438454.00	4153130.01	–0.81	0.16	4.62	0.18
EIIV	Y	Catania	507254.31	4151853.86	0.31	0.09	3.01	0.12
GALF	N[2]	Gagliano (EN)	461792.51	4173805.69	–1.98	4.71	0.25	0.10
HAGA	Y	Augusta (SR)	513742.47	4126595.04	–0.93	0.08	5.17	0.07
HAV1	Y	Avola (SR)	510852.78	4090415.57	–1.12	0.09	5.27	0.09
HCRL	Y	Carlentini (SR)	502871.55	4126273.23	–0.02	0.26	3.68	0.24
HLNI	Y	Lentini (SR)	488658.55	4133547.84	–1.02	0.05	4.57	0.09
HMDC	Y	Ragusa	480692.22	4090348.32	–1.01	0.08	4.99	0.08
HPAC	Y	Pachino (SR)	503323.40	4062537.44	–1.18	0.18	5.40	0.16
HSCI	Y	Scicli (RG)	473817.55	4072038.75	–0.91	0.05	4.72	0.05
HVZN	Y	Vizzini (CT)	474742.47	4114695.12	–1.84	0.16	4.90	0.12
NOT1	Y	Noto (SR)	499090.21	4081099.92	–1.45	0.09	5.32	0.07
POZL	Y	Modica (RG)	481574.75	4064773.79	–1.05	0.05	5.06	0.09
RAFF	Y	Mazzarino (CL)	443431.79	4119752.93	–1.49	0.08	4.97	0.09
SSYX	Y	Sortino (SR)	506780.26	4112360.40	–1.18	0.08	4.76	0.08

[1] Provinces: Agrigento (AG); Caltanissetta (CL); Catania (CT); Enna (EN); Ragusa (RG); Siracusa (SR).
[2] Station not used because velocity changed with the time (the partial time series are not enough long).

Table 1. GNSS stations considered for velocity and strain rate computation. Only time series having at least 4.5 y duration are shown.
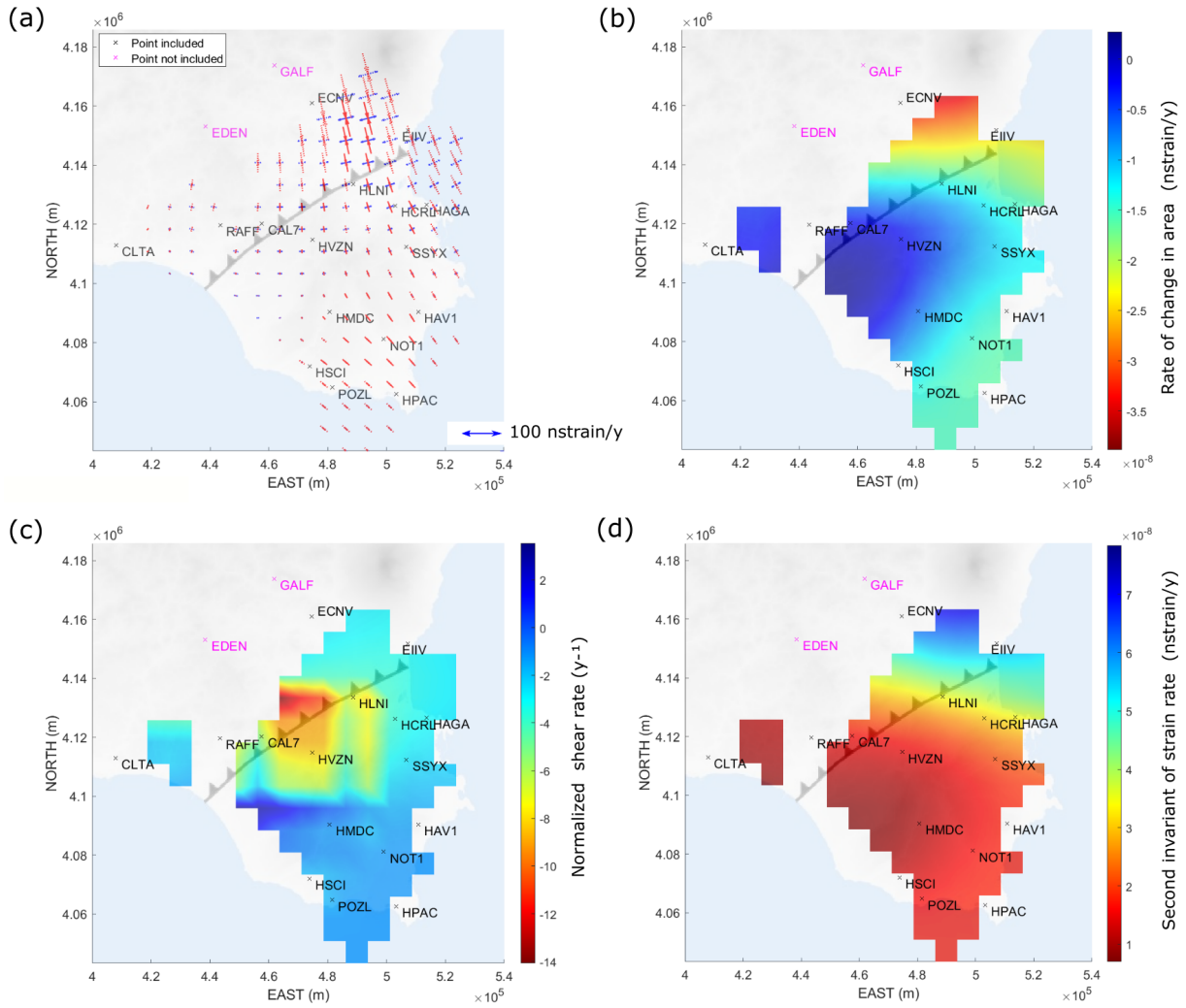
Figure 7. Strain rate field for 28-km scale factor: (a) strain tensors (solid line: data in high significance areas; dotted lines: data in mean significance areas); (b) map of change in area rate (dilatation rate); (c) map of engineering shear rate, normalized to dilatation; (d) map of second invariant of the strain rate.

(ii) the North-West one (NW), with the stations CAL7, CLTA and RAFF, where compression prevails by a factor 2 but do not exceed 20 nstrain/y;

(iii) the South-East area (SE), with the stations HAGA, HCRL and SSYX, where compression still prevails by a factor 2 and reaches 30 nstrain/y;

(iv) the South-West are (SW), with HVZN, which is the only zone were extension and compression are similar and are about 10 nstrain/y;

(v) the extreme south portion, with the stations HAV1, HMDC, HPAC, HSCI, NOT1 and POZL, where the compression reaches about 20 nstrain/y with azimuth of about 45°.

The results generally agree with the map of geodetic horizontal strain rate in Italy provided by Mattia et al. [2012] and Palano [2015]. In particular, the principal directions of the strain rate are completely in agreement. There is a discrepancy between the values, even though the orders of magnitude are correct. However, it is noted that as the scale factor decreases, and therefore as the number of stations that influence the calculation of the strain rate in a grid node decreases, the strain rate in the NE area tends to increase and therefore to approach that estimated by Mattia et al. [2012] and Palano [2015]. However, the reduction of the scale factor also entails the reduction of the geometric significance of the results (only the grid nodes surrounded by stations on at least two sides are really significant) and therefore it is not possible to further reduce the scale factor. Various authors who studied the area

also used data supplied by non-permanent stations or in any case by stations whose data were not accessible for this calculation. This also explain the small discrepancy between the obtained values of strain rate in this study if compared to previous investigations. It is important to underline that the reduction of the scale factor has no significant effect on the results obtained in the NW, SE, SW and ES areas.

In the specific case, CME filtering has no effect on the results, as expected due to the relatively limited size of the area and the fact that only the 2D deformation is studied, with no interest in the vertical component.

Area			Scale factor (km)		
			28	**24**	**20**
NE	$\dot{\varepsilon}_{max}, \dot{\varepsilon}_{min}, \varphi$ (nstrain/y, °)	mean	$29 \pm 5, -75 \pm 16, 75°$	$34 \pm 6, -83 \pm 22, 77°$	$38 \pm 9, -90 \pm 27, 77°$
		extreme	$23 \pm 13, -99 \pm 10, 82°$	$26 \pm 13, -120 \pm 10, 82°$	$35 \pm 13, -140 \pm 8, 81°$
NW	$\dot{\varepsilon}_{max}, \dot{\varepsilon}_{min}, \varphi$ (nstrain/y, °)	mean	$8 \pm 3, -14 \pm 6, -70°$	$8 \pm 2, -17 \pm 5, -60°$	$7 \pm 2, -20 \pm 10, -61°$
		extreme	$9 \pm 3, -19 \pm 10, -80°$	$10 \pm 5, -16 \pm 7, -88°$	$9 \pm 3, -19 \pm 10, -84°$
SE	$\dot{\varepsilon}_{max}, \dot{\varepsilon}_{min}, \varphi$ (nstrain/y, °)	mean	$12 \pm 5, -21 \pm 8, 70°$	$10 \pm 5, -18 \pm 8, 70°$	$14 \pm 6, -21 \pm 9, 68°$
		extreme	$17 \pm 5, -24 \pm 5, 76°$	$20 \pm 5, -32 \pm 5, 70°$	$23 \pm 3, -35 \pm 5, 70°$
SW	$\dot{\varepsilon}_{max}, \dot{\varepsilon}_{min}, \varphi$ (nstrain/y, °)	mean	$6 \pm 2, -5 \pm 3, 80°$	$7 \pm 3, -4 \pm 3, 80°$	$7 \pm 3, -4 \pm 3, 80°$
		extreme	$9 \pm 5, -7 \pm 4, 83°$	$12 \pm 5, -11 \pm 5, 80°$	$13 \pm 5, -11 \pm 5, 84°$
ES	$\dot{\varepsilon}_{max}, \dot{\varepsilon}_{min}, \varphi$ (nstrain/y, °)	mean	$1.3 \pm 0.5, -16 \pm 3, 45°$	$1.5 \pm 0.8, -16 \pm 3, 47°$	$1.3 \pm 0.9, -18 \pm 9, 46°$
		extreme	$0.7 \pm 0.5, -18 \pm 1, 45°$	$1.0 \pm 0.8, -18 \pm 1, 43°$	$1.0 \pm 0.9, -19 \pm 1, 41°$

Table 2. Results of strain rate calculation in some areas with respect to the Main Thrust Fault: North-East (NE), North-West (NW), South-East (SE), South-West (SW), extreme South (ES) for three values of scale factor.

4. Discussion

This research aims to provide a free toolbox for immediate use by users interested in calculating crustal deformation in an area for which the time series of the coordinates of some continuous GNSS stations are available. The two components of the toolbox, i.e. StaVel for the velocity computation from the station coordinates, and GridStrain for the strain rate computation from the station velocities, are designed to be used together, but they are standalone programs which can be used separately.

It is necessary to underline that, even if the toolbox is designed to operate with a high degree of automation, it requires manual verification of the plausibility of the results. In particular, it is necessary to verify that the offsets in the time series are correctly recognized. Any offsets not recognized automatically can be recognized manually using a StaVel function that allows the user to view the time series and zoom in on them. The development of a method, based on deep learning, aimed at automatically recognizing offsets with high reliability is currently underway. It is important to underline that any app or software package, however advanced, is a tool in the hands of the researcher and the results must always be critically assessed. StaVel allows the check of each stage of data processing aimed

at obtaining the velocities, offering the possibility to intervene where necessary. It is no accident that the options of the main function of StaVel (Figure 4) allow the user to modularize the various phases of data processing, so as to allow the user to control, if desired, each of them. Moreover, GridStrain allows the user to choose the scaling function and, above all, the scale factor, in order to choose the locality level of the strain calculation.

Results from South-Eastern Sicily confirm that the known kinematics can be reproduced by means of the proposed toolbox. The expected behaviors (compressive or extensive) are well identified and the orders of magnitude of the obtained values are correct. The case study highlights the importance of the possible choice of one or more scale factors. The fact that by decreasing the scale factor there are no variations of the estimated values in the NW, SE, SE and ES areas, while an increase of the compression is observed in the NE area, reaching values ever closer to the Mattia et al. [2012] ones, shows that the NGL database is not sufficient to fully study the NE, which is a zone particularly interesting due to the corresponding high strain rate. Not surprisingly, various authors also use data from epGNSS or in any case from other stations. The latter becomes crucially important when geodetic measurements are used, within multidisciplinary approaches considering other constraints (geological, geophysical, geochemical, etc), to improve the seismic hazard assessment of regions prone to damaging earthquakes, as pointed out e.g. by Meschis et al. [2022], Mildon et al. [2022] and Robertson et al. [2020].

The approach implemented in StaVel is not suitable if epGNSS data are use, i.e. if the data are periodically acquired through specific measurement campaigns. This because, in those cases, periodic components and noise cannot be adequately modeled and the velocity uncertainties could be underestimated. The Monte Carlo approach for the estimation of reasonable thresholds for epGNSS velocity errors proposed by Pesci et al. [2009] and implemented, with some variations, in SURMODERR MATLAB toolbox [Teza et al., 2010], should be used instead. In the event that there are also epGNSS stations, velocities and corresponding uncertainties must be appended to the text file generated by StaVel before the use of GridStrain.

The time necessary to calculate the velocities of 18 GNSS stations, is about two hours using a notebook equipped with a 11th Gen Intel® Core® i7-1165G7 CPU with 2.80 GHz clock, 16 GB RAM. The time required to verify the time series, in particular to verify that the offsets are correctly identified and, if necessary, corrected in a manual way is approximately 2 h. The CME estimation and filtering require a few minutes. The computation of the strain rate field can be carried out in a few minutes for each scale factor. The toolbox can therefore be used with resources typically available today.

5. Conclusions

In conclusion, a flexible toolbox, which is the evolution of a previous one [Teza et al., 2008], was developed. It requires data easily available in the geodetic data repositories (e.g. the NGL one) and provides the velocities and strain rates. The computation cost is reasonable and compatible with standard computing resources.

Last but not least, the fact that the code is developed according to the object-oriented programming paradigm and is fully accessible makes it compatible with Python and also convertible to Python, i.e. a license-free software.

Data and sharing resources. The code related to this paper, including all functions, StaVel and GridStrain user's guides and tutorial data, is available at Harvard Dataverse and, when necessary, will be updated. Download links: https://doi.org/10.7910/DVN/9XV3K2 (StaVel); https://doi.org/10.7910/DVN/VQS0CO (GridStrain).

References

Alothman, A., R.M. Fernandes, M.S. Bos, S. Schillak and B. Elsaka (2016). Angular velocity of Arabian plate from multi-year analysis of GNSS data, Arab. J. Geosci., 9, 8, 1-10, https://doi.org/10.1007/s12517-016-2569-5.

Blewitt, G., C. Kreemer, W.C. Hammond and J. Gazeaux (2016). MIDAS robust trend estimator for accurate GPS station velocities without step detection. J. Geophysical Res.: Solid Earth, 121, 2054-2068, https://doi.org/10.1002/2015JB012552.

Blewitt, G., W.C. Hammond and C. Kreemer (2018). Harnessing the GPS data explosion for interdisciplinary science, Eos, 99, ht tps://doi.org/10.1029/2018EO104623.

Boehm, J., B. Werl and H. Schuh (2006). Troposphere mapping functions for GPS and very long baseline interferometry from European Centre for Medium-Range Weather Forecasts operational analysis data, J. Geophysical Res., 111, B02406, https://doi.org/10.1029/2005JB003629.

Bos, M.S., R.M.S. Fernandes, S.D.P. Williams and L. Bastos (2013). Fast error analysis of continuous GNSS observations with missing data, J. Geod., 87, 351-360, https://doi.org/10.1007/s00190-012-0605-0.

Dmitrieva, K., P. Segall, and C. DeMets (2015). Network-based estimation of time-dependent noise in GPS position time series, J. Geod., 89, 591-606. https://doi.org/10.1007/s00190-015-0801-9.

Farr, T.G., P.A. Rosen, E. Caro, R. Crippen, R. Duren, S. Hensley, M. Kobrick, M. Paller, E. Rodriguez, L. Roth, D. Seal, S. Shaffer, J. Shimada, J. Umland, M. Werner, M. Oskin, D. Burbank, and D. Alsdorf (2007). The Shuttle Radar Topography Mission, Rev. Geophys., 45, RG2004, https://doi.org/10.1029/2005RG000183.

Gazeaux, J., S. Williams, M. King, M. Bos, R. Dach, M. Deo, A.W. Moore, L. Ostini, E. Petrie, M. Roggero, F.N. Teferle, G. Olivares and F.H. Webb (2013). Detecting offsets in GPS time series: First results from the detection of offsets in GPS experiment, J. Geophysical Res.: Solid Earth, 118(5), 2397-2407, https://doi.org/10.1002/jgrb.50152.

Gruszczynski, M., A. Klos, and J. Bogusz (2016). Orthogonal transformation in extracting of common mode error from continuous GPS networks. Acta Geodyn. et Geomater., 13, 291-298, https://10.13168/AGG.2016.0011.

He, X., K. Yu, J.-P. Montillet, C. Xiong, T. Lu, S. Zhou, X. Ma, H. Cui and F. Ming (2020). GNSS-TS-NRS: An Open-Source MATLAB-based GNSS time series noise reduction software, Remote Sens., 12, 3532, https://doi.org/10.3390/rs12213532.

Ji, K. and Y. Shen (2020). A wavelet-based outlier detection and noise component analysis for GNSS position time series, in International Association of Geodesy Symposia, 1-9, Springer, Berlin, Heidelberg, 44-53, https://doi.org/10.1007/1345_2020_106.

Kenyeres, A., J.G. Bellet, C. Bruyninx, A. Caporali, F. de Doncker, B. Droscak, A. Duret, P. Franke, I. Georgiev, R. Bingley, L. Huisman, L. Jivall, O. Khoda, K. Kollo, A.I. Kurt, S. Lahtinen, J. Legrand, B. Magyar, D. Mesmaker, K. Morozova, J. Nágl, S. Özdemir, X. Papanikolaou, E. Parseliunas, G. Stangl, M. Ryczywolski, O.B. Tangen, M. Valdes, J. Zurutuza, and M. Weber (2019). Regional integration of long-term national dense GNSS network solutions, GPS Solut., 23(4), 122, https://doi.org/10.1007/s10291-019-0902-7.

Kierulf, H.P. (2017). Analysis strategies for combining continuous and episodic GNSS for studies of neo-tectonics in Northern-Norway, J. Geodyn. 109, 32-40, https://doi.org/10.1016/j.jog.2017.07.002.

Klos, A., J. Bogusz, M. Figurski and W. Kosek (2015). On the Handling of Outliers in the GNSS Time Series by Means of the Noise and Probability Analysis, Cent. Eur. J. Geosci., 143, 657-664, https://doi.org/10.1007/1345_2015_78.

Kreemer, C., G. Blewitt and E.C. Klein (2014). A geodetic plate motion and Global Strain Rate Model, Geochem. Geophys. Geosystems, 15, 3849-3889, https://doi.org/10.1002/2014GC005407.

Langbein, J. (2004). Noise in two-color electronic distance meter measurements revisited, J. Geophysical Res., 109(B4), B04406, 1-16. https://doi.org/10.1029/2003JB002819.

Langbein, J. and Y. Bock (2004). High-rate real-time GPS network at Parkfield: Utility for detecting fault slip and seismic displacements, Geophys. Res. Lett., 31, L15S20, https://doi.org/10.1029/2003GL019408.

Langbein, J. (2020). Methods for rapidly estimating velocity precision from GNSS time series in the presence of temporal correlation: a new method and comparison of existing methods. J. Geophysical Res.: Solid Earth, 125, e2019JB019132, https://doi.org/10.1029/2019JB019132.

Legrand J. (2022). EPN multi-year position and velocity solution CWWWW, Royal Observatory of Belgium, available online at https://doi.org/10.24414/ROB-EUREF-CWWWW (accessed 10 July 2022).

Li, W., W. Jiang, Z. Li, H. Chen, Q. Chen, J. Wang and G. Zhu, G. (2020). Extracting common mode errors of regional GNSS position time series in the presence of missing data by variational bayesian principal component analysis, Sensors, 20, 8, 2298, https://doi.org/10.3390/s20082298.

Mao, A., C.G.A. Harrison and T.H. Dixon (1999). Noise in GPS coordinate time series, J. Geophysical Res., 104, B2, 2797-2816, https://doi.org/10.1029/1998JB900033.

Masson, C., S. Mazzotti and P. Vernant (2019). Precision of continuous GPS velocities from statistical analysis of synthetic time series, Solid Earth, 10, 329-342, https://doi.org/10.5194/se-10-329-2019.

Mattia, M., V. Bruno, F. Cannavò and M. Palano (2012). Evidences of a contractional pattern along the northern rim of the Hyblean plateau (Sicily, Italy) from GPS data, Geol. Acta, 10, 1, 63-70, https://doi.org/10.1344/105.000001705.

Meschis, M., G. Scicchitano, G.P. Roberts, J. Robertson, G. Barreca, C. Monaco, C. Spampinato, D. Sahy, F. Antonioli, Z.K. Mildon and G. Scardino (2020). Regional deformation and offshore crustal local faulting as combined processes to explain uplift through time constrained by investigating differentially uplifted late quaternary

paleoshorelines: the Foreland Hyblean Plateau, SE Sicily, Tectonics, 39, e2020TC006187, https://doi.org/10.1029/2020TC006187.

Meschis, M., G. Teza, E. Serpelloni, L. Elia, G. Lattanzi, M. Di Donato and S. Castellaro (2022). Refining rates of active crustal deformation in the upper plate of subduction zones, implied by geological and geodetic data: the E-dipping West Crati fault, Southern Italy, Remote Sens., 14, 5303, https://doi.org/10.3390/rs14215303.

Mildon, Z.K., G.P. Roberts, J.P. Faure Walker, J. Beck, I. Papanikolaou, A.M., Michetti, S. Toda, F. Iezzi, L. Campbell, K.J.W. McCaffrey, R. Shanks, C. Sgambato, J. Robertson, M. Meschis and E. Vittori (2022). Surface faulting earthquake clustering controlled by fault and shear-zone interactions, Nat. Commun., 13, 1, 7126, https://doi.org/10.1038/s41467-022-34821-5.

Nikolaidis, R. (2002). Observation of Geodetic and Seismic Deformation with the Global Positioning System. PhD dissertation, University of California: San Diego, CA, USA, available online at: https://www.proquest.com/pagepdf/304798351?accountid=9652 (last access: 16/11/2022).

NOAA National Geodetic Survey (1994). NOAA Archive of NGS National Continuously Operating Reference Station (CORS) Network (NCN), NOAA National Centers for Environmental Information, available online at https://doi.org/10.25921/wc4r-ee36 (accessed 10 October 2022).

Ohta, Y. and M. Ohzono (2022). Potential for crustal deformation monitoring using a dense cell phone carrier Global Navigation Satellite System network, Earth Planets Space, 74, 25, https://doi.org/10.1186/s40623-022-01585-7.

Palano, M. (2015). On the present-day crustal stress, strain-rate fields and mantle anisotropy pattern of Italy, Geophys. J. Int., 200, 2, 969-985, https://doi.org/10.1093/gji/ggu451.

Pesci, A., G. Teza and G. Casula (2009). Improving strain rate estimation from velocity data of non-permanent GPS stations: the Central Apennine study case (Italy), GPS Solut., 13, 4, 249-261, https://doi.org/10.1007/s10291-009-0118-3.

Pintori, F., E. Serpelloni and A. Gualandi (2022). Common-mode signals and vertical velocities in the greater Alpine area from GNSS data, Solid Earth, 13, 10, 1541-1567, https://doi.org/10.5194/se-13-1541-2022.

Ray, J., Z. Altamimi, X. Collieux and T. van Dam (2008). Anomalous harmonics in the spectra of GPS position estimates, GPS Solut., 12, 1, 55-64, https://doi.org/10.1007/s10291-007-0067-7.

Robertson, J., G.P. Roberts, F. Iezzi, M. Meschis, D.M. Gheorghiu, D. Sahy, C. Bristow and C. Sgambato (2020). Distributed normal faulting in the tip zone of the South Alkyonides Fault System, Gulf of Corinth, constrained using ^{36}Cl exposure dating of late-Quaternary wave-cut platforms, J. Struct. Geol., 136, 104063, https://doi.org/10.1016/j.jsg.2020.104063.

Serpelloni, E., A. Cavaliere, L. Martelli, F. Pintori, L. Anderlini, A. Borghi, D. Randazzo, S. Bruni, R. Devoti, P. Perfetti and S. Cacciaguerra (2022). Surface velocities and strain-rates in the Euro-Mediterranean region from massive GPS data processing, Front. Earth Sci., 10:907897, https://doi.org/10.3389/feart.2022.907897.

Shen, Z.-K. and D.D. Jackson (2000). Optimal estimation of geodetic strain rates from GPS data, EOS, Transactions American Geophysical Union, 81, 19, S406.

Shen, Z.-K., D.D. Jackson and B.X. Ge (1996). Crustal deformation across and beyond the Los Angeles basin from geodetic measurements, J. Geophys. Res., 101, 12, 27957-27980, https://doi.org/10.1029/96JB02544.

Snay, R.A. and T. Soler (2008). Continuously Operating Reference Station (CORS): History, applications, and future enhancements, J. Surv. Eng., 134, 4, 95-104, https://doi.org/10.1061/(ASCE)0733-9453(2008)134:4(95).

Teza, G., A. Pesci and G. Casula (2010). SURMODERR: A MATLAB toolbox for estimation of velocity uncertainties of a non-permanent GPS station, Comput. Geosci., 36, 8, 1033-1041, https://doi.org/10.1016/j.cageo.2010.03.003.

Teza, G., A. Pesci, A. and A. Galgaro (2008). Grid_strain and grid_strain3: software packages for strain field computation in 2D and 3D environment, Comput. Geosci., 34, 9, 1142-1153, https://doi.org/10.1016/j.cageo.2007.07.006.

Tian, Y. and Z. Shen (2011). Correlation Weighted Stacking Filtering of Common-Mode Component in GPS Observation Network, Acta Seismol. Sin., 33, 198-208, https://doi.org/10.3969/j.issn.0253-37822011.02.007.

Tsuji, H., Y. Hatanaka, Y. Hiyama, K. Yamaguchi, T. Furuya, S. Kawamoto and Y. Fukuzaki (2017). Twenty-Year Successful Operation of GEONET, Bulletin of the Geospatial Information Authority of Japan, 65, 19-44, Available online at https://jglobal.jst.go.jp/en/detail?JGLOBAL_ID=201802268889248505 (accessed 10 July 2022).

Wdowinski, S., Y. Bock, J. Zhang, P. Fang and J. Genrich (1997). Southern California permanent GPS geodetic array: Spatial filtering of daily positions for estimating coseismic and postseismic displacements induced by the 1992 Landers earthquake, J. Geophysical Res.: Solid Earth, 102, 18057-18070, https://doi.org/10.1029/97JB01378.

Williams, S.D.P. (2003). Offsets in global positioning system time series, J. Geophysical Res., 108, B6, 2310, 1-13, https://doi.org/10.1029/2002JB002156.

Williams, S.D.P. (2008). CATS: GPS coordinate time series analysis software, GPS Solut., 12(2), 147-153, https://doi.org/10.1007/s10291-007-0086-4.

Williams, S.D.P., Y. Bock, P. Fang, P. Jamason, R.M. Nikolaidis, L. Prawirodirdjo, M. Miller and D.J. Johnson (2004). Error analysis of continuous GPS position time series, J. Geophysical Res., 109, B3, B03412, 1-19, https://doi.org/10.1029/2003JB002741.

*CORRESPONDING AUTHOR: Giordano TEZA,
Alma Mater Studiorum University of Bologna, Department of Physics and Astronomy, Viale Berti Pichat 6/2, Bologna 40127, Italy
e-mail: giordano.teza@gmail.com.